Nevada Bureau of Mines and Geology Open-File Report 2022-10

LIDAR MAPPING AND FIELD OBSERVATIONS ALONG THE MOUNT CALLAGHAN FAULTS, CENTRAL NEVADA

Rich D. Koehler
Nevada Bureau of Mines and Geology, University of Nevada, Reno

2022

nbmg Nevada Bureau of Mines and Geology
nbmg.unr.edu

University of Nevada, Reno

NEVADA BUREAU OF MINES AND GEOLOGY OPEN-FILE REPORT 2022-10

Lidar Mapping and Field Observations along the Mount Callaghan Faults, Central Nevada

by

Rich D. Koehler

Nevada Bureau of Mines and Geology, University of Nevada, Reno

2022

Suggested citation:
Koehler, R.D., 2022, Lidar mapping and field observations along the Mount Callaghan faults, central Nevada: Nevada Bureau of Mines and Geology Open-File Report 2022-10, 15 p.

© Copyright 2022 The University of Nevada, Reno.
All Rights Reserved.

INTRODUCTION

This report presents the findings of a reconnaissance lidar and field assessment of the Mount Callaghan faults conducted by the Nevada Bureau of Mines and Geology through a scientific research agreement with Renaissance Exploration, Inc. (Orogen Royalties). The project site is located along the eastern margin of the Toiyabe Range in Lander County, Nevada. Specifically, the site is within the Mount Callaghan and Grass Valley Ranch 7.5' topographic quadrangles, approximately 25 km northeast of Austin, Nevada within southern Grass Valley (fig. 1). The project area is accessed from Grass Valley Road, which extends north from U.S. Highway 50 near Bob Scotts Summit and Callaghan Creek Road, a dirt road associated with Grass Valley Ranch. The site is characterized by a subdued range front and gently east-sloping alluvial fans of various ages incised by narrow alluvial valleys (fig. 2). Isolated knobs of bedrock in the south-central part of the property crop out above the alluvial cover consistent with long-term tectonic activity.

The purpose of the project was to map and characterize Quaternary active fault structures associated with the Mount Callaghan fault system. In particular, the mapping focused on defining the distribution, extent, and orientation of faults, and the width and style of deformation. The results are intended to refine previous fault mapping at the site and inform local and regional subsurface structural modeling useful in future assessments of gold mineralization at depth. Subsequent to the start of the project, high-resolution topographic data (lidar) was collected (5/19/2022) and processed by NV5 Geospatial. The data yielded an elevation point cloud with an average pulse density of ≥8 pulses/m^2 (nominal pulse spacing of 0.35 m) across the 8,535-acre project area that was delivered to Orogen Royalties as a digital elevation model (DEM) and several derivative raster files (e.g., highest hit, intensity, etc.).

The scope of the investigation included a review of previous geologic mapping, review of previous data related to active tectonic faults in the project area, inspection of aerial photographs and lidar data to evaluate site geomorphology and the presence or absence of Quaternary active faults, mapping the surface expression of active faults, field verification, and the dissemination of project results to Orogen Royalties in this report. As part of the scientific research agreement, a graduate student was trained in fault evaluation and documentation techniques.

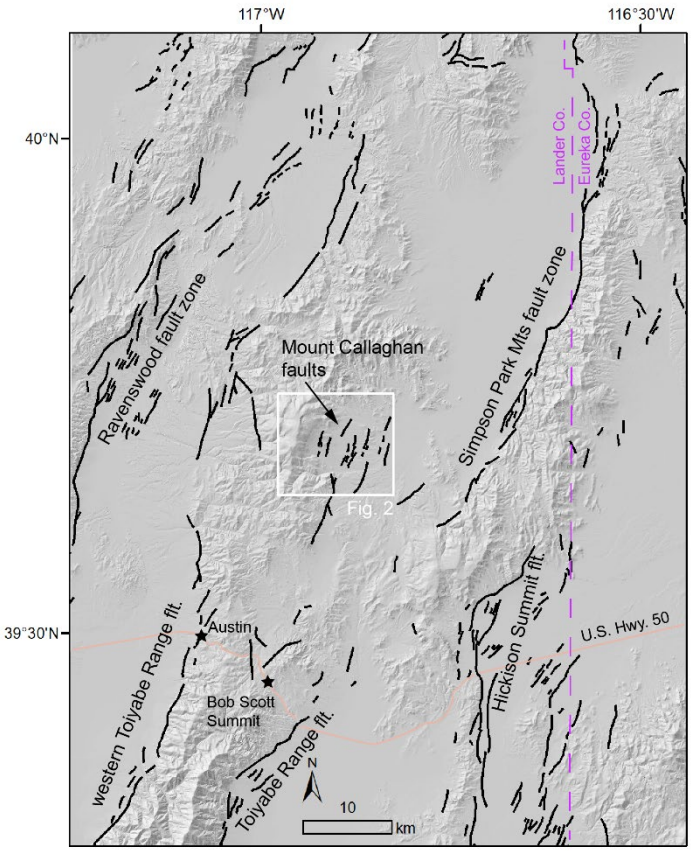

Figure 1. Map showing the tectonic setting of the Mount Callaghan faults project region. Project area shown by white rectangle (fig. 2). Base map is digital elevation model from Shuttle Radar Topography Mission (SRTM, 2013). Faults (black lines) taken from the U.S. Geological Survey Quaternary fault and fold database (USGS, 2022).

ACTIVE FAULTING AND GOLD MINERALIZATION

In Nevada, the basin-and-range topography is generated by active normal faulting along range-front fault systems. Many of these range-front fault systems are associated with scarps in Quaternary deposits indicating relatively youthful displacements. Patterns of microseismicity indicate that tectonic deformation is distributed throughout the state, with >15,000 earthquakes recorded each year (Anderson et al., 2019). Geodetic and geologic studies indicate that the style of deformation across central and eastern Nevada is dominated by ~1–2 mm/yr of extension oriented N55°W (Hammond et al., 2014; Hammond and Thatcher, 2004; Koehler and Wesnousky, 2011). Although deformation is widely distributed, large magnitude (M≥6.0–6.5) surface-rupturing earthquakes (typically 20–76 km in length) are usually associated with well-defined faults with mappable surface traces. These

earthquakes rupture through the seismogenic crust into the brittle ductile transition zone influencing fluid flow and permeability over large areas. Thus, understanding the distribution of these active fault systems, their interaction with ancient shear zones, as well as their kinematics can provide insight for understanding the distribution of gold mineralization at depth.

Earthquake behavior along active fault zones has been shown to localize fluid migration and influence the generation of fault-related gold deposits (Cox, 2005; Sibson et al., 1988). In contrast to relatively long unmineralized regional-scale fault structures, mineralization more typically occurs along small-displacement faults and shear zones (Eisenlohr et al., 1989). Coulomb stress transfer modeling of mineralized fossil fault systems indicates that gold deposits are spatially correlated with the occurrence of repeated aftershock clusters along active fault systems, often at the ends of fault segments (Cox and Ruming, 2004; Micklethwaite and Cox, 2004; 2006). Aftershocks that are associated with small-displacement rupture on subsidiary faults within earthquake damage zones, increase permeability through the depth of the crust, and may trigger re-activation of pre-existing shear zones (Micklethwaite, 2007; Kilb and Rubin, 2002; Beroza and Zoback, 1993). These processes are important for understanding the distribution of gold deposits, because they create favorable conditions for fluid-rock interaction, fluid mixing, and the migration of mineralization.

The patterns of active faulting and its association with geothermal activity has been evaluated in Nevada as part of regional assessments of the location of geothermal systems (Faulds et al. 2021). That study determined that geothermal systems commonly occur in favorable structural settings associated with fault step-overs or relay ramps, normal fault terminations, fault intersections, accommodation zones, and displacement transfer zones, among several other less common settings. These complex tectonic settings correspond to long-term, critically stressed areas, where fluid pathways are more likely to remain open in networks of closely spaced breccia-dominated fractures, which facilitate fluid migration and the existence of geothermal systems (Faulds et al., 2021). Tectonic and thermo-geologic settings conducive to geothermal activity (e.g., fractured permeable rock) are similar to the types of settings that control fault-related gold mineralization. Thus, documenting the location of active faults in these types of settings has the potential to guide future gold exploration.

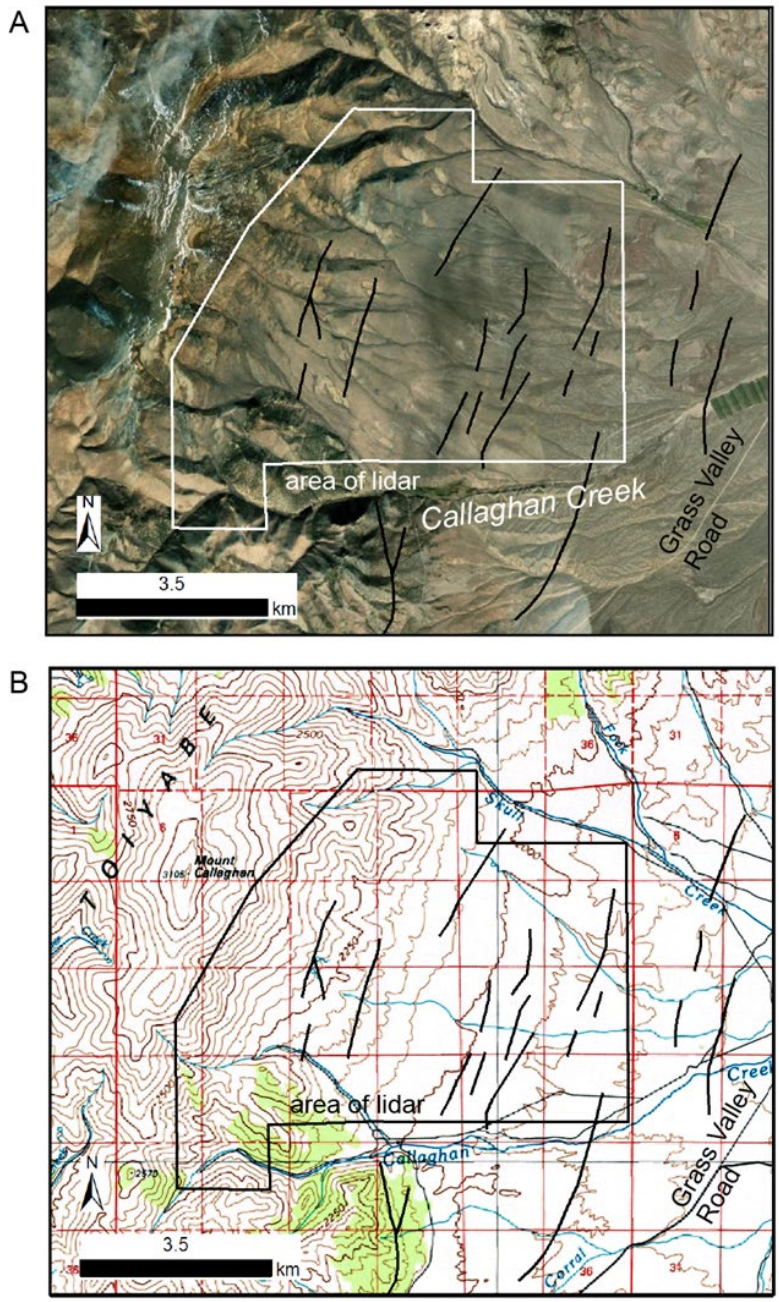

Figure 2. Maps of the project area including (A) Satellite imagery and (B) topography from the Simpson Park Mountains 1:100,000-scale topographic quadrangle. Outline of lidar data used in this project shown by white outline in (A) and black outline in (B). Faults (black lines) taken from the U.S. Geological Survey Quaternary fault and fold database (USGS, 2022).

REVIEW OF PREVIOUS WORK ON THE MOUNT CALLAGHAN FAULTS AND OTHER QUATERNARY FAULTS IN THE PROJECT AREA

Active tectonic faults in the project region that have generated surface-rupturing earthquakes in the Quaternary include the Toiyabe Range, western Toiyabe Range, Hickison Summit, Simpson Park Mountains, and Ravenswood fault systems (fig. 1). These faults all extend along the base of mountain ranges and together accommodate part of the ~1–2 mm/yr of crustal extension responsible for the evolution of the modern Basin and Range topography. Although the surface traces of these faults have been relatively well documented (Stewart and McKee, 1968; 1977; Stewart and Carlson, 1976; Dohrenwend et al., 1992; Schell, 1981; Roberts et al., 1963), few detailed studies have been conducted, and information on their slip rate, rupture history, recurrence behavior, and maximum earthquake potential, as well as their structural complexities at depth are not well-constrained. The existence of the McGinness Hills geothermal power plant south of the project area provides evidence of complex kinematic fault linkages at depth. Based on these linkages and their potential influence on gold mineralization, a review of previous mapping and the general Quaternary tectonic characteristics of faults in the near-field project area is provided below.

The Mount Callaghan faults occur along the eastern flank of the northern Toiyabe Range and extend across a small range-front embayment in southwestern Grass Valley (figs. 1 and 2). Geologic maps produced by Stewart and Carlson (1976) and Stewart and McKee (1968; 1977) show a buried fault along a short section of the range front in the project area. These maps also depict several parallel approximately located faults east of the range front cutting older alluvial (QToa) and silicic ash-flow tuff (Tt_2, Tbm) deposits. Stewart and McKee (1977) correlated the ash-flow

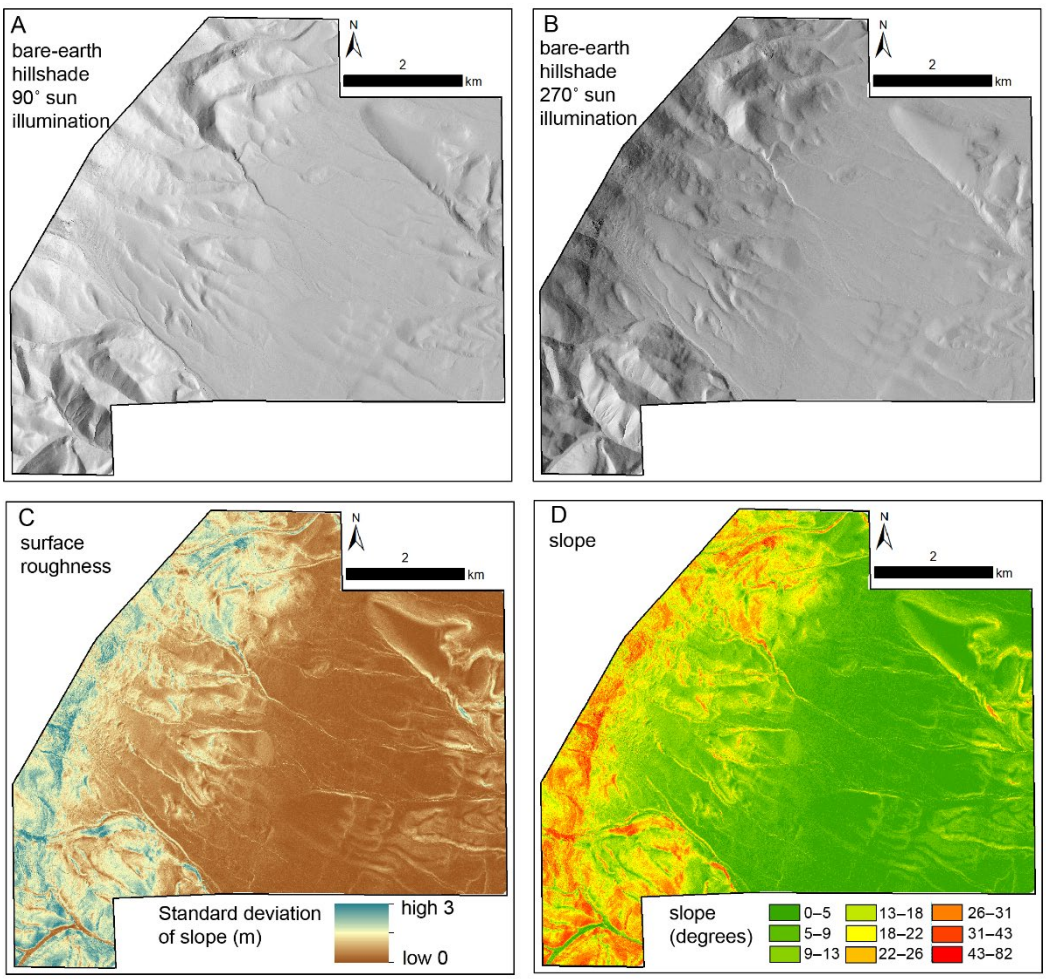

Figure 3. Lidar derivative map products including bare-earth hillshades with 90°(A) and 270° (B) sun illumination angles, surface roughness (C) and slope (D) for the Mount Callaghan faults study area.

tuff to the Bates Mountain Tuff that was dated by K-Ar methods at 23 Ma indicating that deformation post-dates the early Miocene. These maps also show several scarps in alluvium ~3 km south of the project area, but only Stewart and McKee (1968) showed a concealed fault extending from these scarps to the southern margin of the project area. Their map and cross section suggest that this concealed fault is part of the Roberts Mountains Thrust in contrast to the interpretation of Dohrenwend et al. (1992) as described below.

Based on the mapping of Dohrenwend et al. (1992), active traces of the fault extend for ~17 km, with an average trend of N16°E, and are distributed across an ~8 km-wide-zone (Dohrenwend et al., 1992). Dohrenwend et al. (1992) showed lineaments and fault traces along the range front in the project area as well as at least five traces extending across piedmont-slope deposits, where they are characterized by both east- and west-facing scarps and lineaments (two of which are east of the project boundary). These traces were inferred to displace alluvial surfaces of early to middle Pleistocene (0.13–1.5 Ma) and Late Pleistocene (<130 ka) age (Dohrenwend et al., 1992). Dohrenwend et al. (1992) also showed a prominent range-front trace extending south of the project boundary consistent with long-term down-to-the-east Quaternary displacement. The fault mapping of Dohrenwend et al. (1992) was incorporated into the U.S. Geological Survey's National Quaternary fault and fold database as shown on figures 1 and 2. Geologic and geodetic modeling in support of the U.S. Geological Survey's 2023 update of the National Seismic Hazards Map (NSHM) assigned a slip rate of 0.076 mm/yr for the Mount Callaghan faults (Hatem et al., 2022).

The east-dipping Toiyabe Range fault extends along the eastern flank of the Toiyabe Range for ~116 km with an average strike of N20°E (Dohrenwend et al., 1992). The northern projection of the fault is within ~15 km of the Mount Callaghan faults and may represent a left step in the range-front fault system (fig. 1). The fault has generated ~1800 m of vertical relief and is clearly expressed along the range front by prominent triangular facets, wineglass canyons, and oversteepened basal slopes. The active trace of the fault is commonly buried by colluvium and young alluvial fans along the bedrock escarpment; however, in several areas the fault projects away from the range front, where it is characterized by multiple overlapping and stepping fault strands, and scarps across late Pleistocene alluvial fans (Koehler, 2009). Paleoseismic trenching studies south of U.S. Highway 50 indicate that the fault has generated at least two late Pleistocene earthquakes associated with ~1.8 m of vertical displacement (Koehler and Wesnousky, 2011). Hatem et al. (2022) determined a slip rate of 0.018 mm/yr for the Toiyabe Range fault.

The northwest-dipping 72-km-long Simpson Park Mountains fault strikes N14°E along the western flank of the Simpson Park Mountains, a structural block consisting of Paleozoic sedimentary and Tertiary volcanic rocks (Dohrenwend et al., 1992; Roberts et al., 1963). The southwestern projection of the fault is within 5 km of the Mount Callaghan faults (fig. 1). Structural relief across the fault is on the order of 1000 m from the highest ridges to the valley floor. Geomorphic evidence of active late Quaternary deformation is expressed along the entire length of the fault, including prominent scarps in alluvial-fan and lacustrine deposits, springs, and vegetation lineaments (Koehler, 2009). Along the central part of the fault near Walti Hot Springs, the highstand shoreline of pluvial Lake Gilbert is displaced ~1.7 m across the fault. A paleoseismic trench and fault scarp diffusion modeling at this site indicated the occurrence of two earthquakes that post-date the highstand (~15,500 cal yr B.P., Adams et al., 2008) with the most recent event around 6.5 ka (Koehler and Wesnousky, 2011). A slip rate of 0.26 mm/yr was determined by Hatem et al. (2022) for the Simpson Park Mountains fault.

LIDAR AND FIELD OBSERVATIONS

Modern satellite imagery, lidar data, and field reconnaissance provide the basis for evaluation of the site geomorphology, detailed mapping of the location of active fault traces, and an assessment of the relative age of fault displacements. To facilitate this analysis, derivative map products were produced from the lidar digital elevation model (DEM) including several bare-earth hillshade models with different sun illumination angles, a surface roughness map (standard deviation of slope), and a slope map (fig. 3). A field photograph of the general study area geomorphology is shown on figure 4.

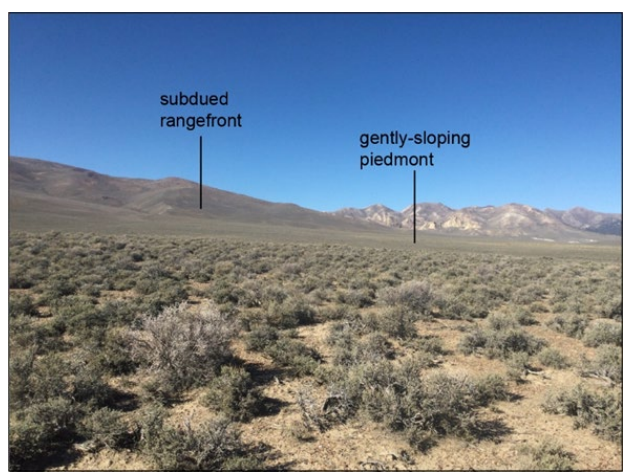

Figure 4. Photograph of the northwestern part of the Mount Callaghan faults study area showing the subdued morphology of the range front and alluvial fans that comprise the gently-sloping piedmont.

Inspection of the lidar derivative maps and field observations indicate that the geomorphology of the project area is characterized by a subdued range front and a gently east-sloping piedmont slope that extends between an elevation of ~2,250 and ~1,850 ft (figs. 2, 3, and 4). Based on the amount of incision, relative elevation of alluvial surfaces above modern stream grade, and crosscutting depositional and inset relations, at least three different ages of Quaternary alluvial surfaces comprise the piedmont slope. The oldest surfaces (Qfo) have been incised to depths of greater than 10 m and are characterized by headwardly eroding channels and rounded interfluves. Intermediate-aged surfaces (Qfi) are inset into Qfo surfaces and have been incised to depths of ~2–6 m. The youngest alluvial surfaces (Qfy) actively bury Qfo and Qfi surfaces near the range front, and incise these surfaces east of the range front where they are characterized by narrow alluvial valleys. Qfy surfaces have a distinct distributary drainage pattern and preserve bar-and-swale morphology. Isolated bedrock knobs occur as outcrops above the alluvial-fan cover in the eastern and northern parts of the study area.

Although the ages of the alluvial surfaces are unknown, their surficial characteristics are similar to alluvial surfaces studied in the region that have been dated by relative (i.e., soils) and absolute (i.e., ^{10}Be and ^{36}Cl cosmogenic and optically stimulated luminescence) dating methods (e.g. Angster et al. 2019, Koehler and Wesnousky, 2011; Wesnousky et al., 2005). Based on these studies, it is inferred that the ages of the Qfo and Qfi surfaces are broadly constrained to greater than several hundred thousand years and ~50–130 ka, respectively. It is also inferred that Qfy surfaces are latest Pleistocene to Holocene in age. These ages are generally consistent with the ages inferred for surfaces on the piedmont by Dohrenwend et al. (1992).

Individual field observations collected during a two-day reconnaissance on October 13 and 14, 2022 that pertain to the location of active faults, scarp heights, and the relative ages of displaced surfaces are summarized in table 1. Additional details and photographs from selected field observation sites are contained in Appendix A. Interpreted locations of active fault traces and the locations of individual field observations are shown on figures 5A and 5B, respectively. Topographic profiles generated from the lidar data were constructed across interpreted fault traces and are shown on figure 6. The reconnaissance included walking transects along several of the identified faults in the southern part of the study area and inspecting the range front from dirt road vantage points (figure 5B). Additionally, drainages that cut across the Mount Callaghan faults were inspected for fault exposures that could provide information on the dip of the fault; however, due to colluvial cover, outcrops of the fault were not observed.

In general, the east-dipping range-front fault within the study area is weakly expressed and lacks tectonic geomorphic features indicative of active tectonic deformation (i.e., triangular facets). Alluvial surfaces on the

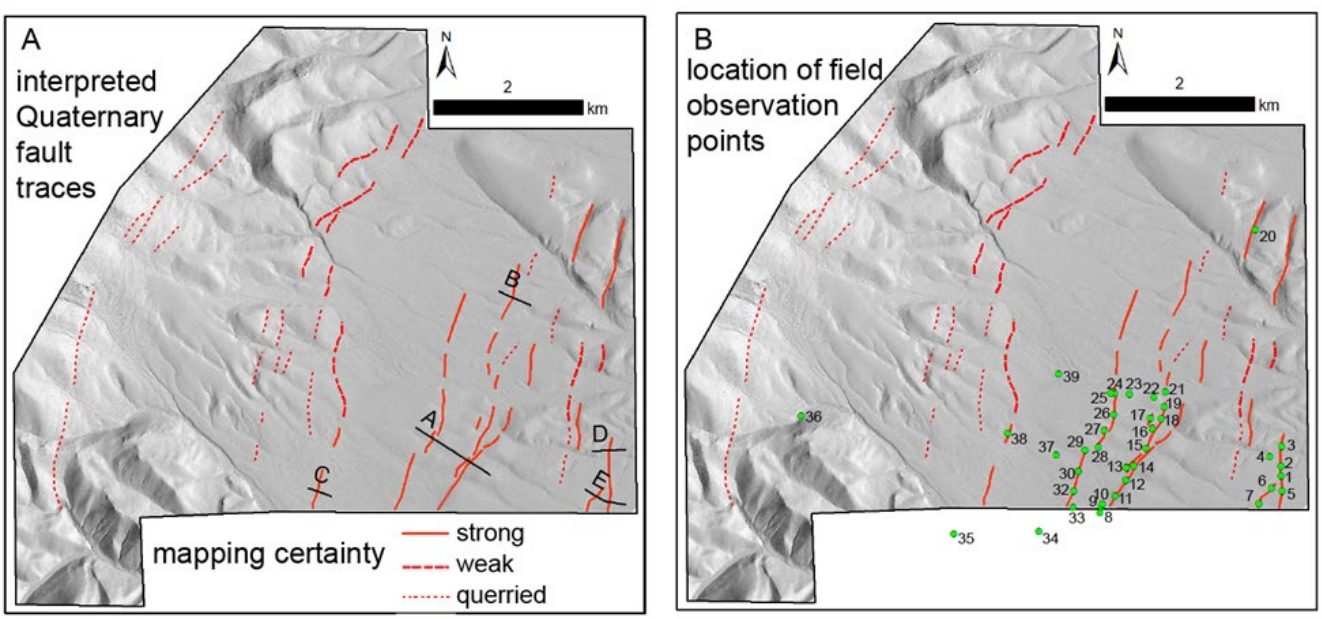

Figure 5. (A) Location of interpreted Quaternary fault traces associated with the Mount Callaghan faults and location of topographic profiles A–E (fig. 6). (B) Location of individual field observation sites (numbered green circles).

Table 1. Field observation site number, location, and observations. Reference to relative alluvial-fan surface age in observations corresponds to young (Qfy), intermediate (Qfi), and old (Qfo). Scarp heights estimated by hand level in the field. Photographs of selected field observation sites are contained in Appendix A.

Field observation location (Site #)	Latitude	Longitude	Observations
1	39.672182	-116.859415	East-facing scarp Qfi surface, scarp height ~1.5 m.
2	39.673326	-116.859505	East-facing scarp, Qfy surface to north not offset. Fault continues on north side of wash across Qfo surface.
3	39.675687	-116.859408	East-facing scarp, scarp height ~3.5 m, scarp continues north of this site.
4	39.674544	-116.861076	Qfy surface. No displacement on surface along fault to the east.
5	39.670537	-116.859233	East-facing scarp on Qfi surface, scarp height ~1.5 m.
6	39.670896	-116.860806	East-facing scarp on Qfi surface, scarp height ~2 m. Scarp has smooth profile.
7	39.668968	-116.862845	East-facing scarp on Qfi surface, scarp height ~2 m. Continuous to Site 6. Qfy surfaces that cut through Qfi are not displaced.
8	39.667779	-116.887649	West-facing scarp, subtle, scarp height ~0.5 m.
9	39.668422	-116.887648	Qfy surface with no observable scarp.
10	39.668923	-116.887462	From this site, a prominent east-facing scarp is observed upslope to the west.
11	39.669993	-116.885332	West-facing scarp in Qfi surface, scarp height ~3 m. Scarp has smooth profile and is well diffused.
12	39.671637	-116.883756	West-facing scarp in Qfi surface continuous to Site 11.
13	39.673210	-116.883661	Vantage point to view west-facing scarp at Site 14.
14	39.673423	-116.882365	West-facing scarp in Qfo surface associated with subtle graben ~100 m wide.
15	39.675639	-116.880510	Graben extending across Qfo surface. Prominent east-facing scarp at Site 15. West- facing scarp at Site 14 projects along east side of graben east of this site.
16	39.677998	-116.879488	East-facing scarp in Qfo surface. A short parallel trace occurs ~15 m upslope of this site (Site 17).
17	39.679214	-116.879948	East-facing scarp in Qfo surface, scarp height ~2 m. Trace is short and discontinuous, upslope of scarp at Site 16.
18	39.679069	-116.878097	East-facing scarp in Qfo surface.
19	39.680427	-116.877632	East-facing scarp in Qfo surface.
20	39.702010	-116.863243	Site observed from Site 19. Apparent west-facing escarpment in bedrock.
21	39.682430	-116.877443	Fault trace buried by Qfy surface.
22	39.681859	-116.879203	Prominent east-facing scarp upslope (Site 24) observed from this vantage point.
23	39.682078	-116.883183	Prominent east-facing scarp upslope (Site 24) observed from this vantage point.
24	39.682366	-116.885496	East-facing scarp in Qfo surface, scarp height ~4 m.
25	39.682224	-116.886145	Range-front upslope of Site 25 characterized by weak tectonic geomorphology, facets and wineglass canyons not present.
26	39.679720	-116.885593	East-facing scarp continuous to Site 24.
27	39.677648	-116.887170	East-facing scarp in Qfo surface, scarp height ~4 m. A short, less prominent, parallel east-facing trace occurs ~15 m to east.
28	39.675718	-116.888006	East-facing scarp in Qfo surface. To south this trace steps to the west and diminishes in height at Site 29.
29	39.675290	-116.890043	East-facing scarp in Qfi(?) surface, scarp height ~1.5 m.
30	39.672717	-116.890973	East-facing scarp in Qfi surface.
31	39.672717	-116.890973	Duplicate recording of Site 30.
32	39.670357	-116.891994	East-facing scarp in Qfi surface, scarp height ~1.5 m.
33	39.668355	-116.891905	Vantage point to view scarps upslope.
34	39.665642	-116.897277	Vantage point to view scarps upslope.
35	39.665295	-116.910510	Prominent escarpment interpreted to be bedrock strath terrace where two stream channels intersect (non-tectonic).
36	39.679615	-116.934557	Vantage point to view escarpment west of range front extending across mountain slope. Interpreted to be a bedrock contact possibly reflecting differential erosion (non-tectonic).
37	39.674794	-116.894579	Vantage point to view scarp upslope at Site 38.
38	39.677518	-116.902257	Prominent east-facing scarp, scarp height ~2.5 m.
39	39.684592	-116.894101	Vantage point to view range-front morphology. Tectonic geomorphic evidence is weak and not indicative of active deformation. Mapped traces considered questionable.
40	39.624012	-116.900783	Vantage point from Grass Valley Road. To west is a prominent range-front trace that projects north towards the Mount Callaghan faults. May represent a left step from the Toiyabe Range fault to the southeast.

piedmont slope are relatively flat and gently east sloping and are cut by fault scarps that range in slope angle from 9° to 18° (fig. 3). Here, traces of the fault are clearly expressed, well-defined, and trend N10°E to N20°E. The faults on the piedmont dip to the east and west and form several parallel grabens that may sole into a master east-dipping fault at depth. The faults also trend across Tertiary tuff deposits consistent with long-term tectonic displacement across the piedmont. Two additional traces mapped by Dohrenwend et al. (1992) that were not visited in the field occur east of the field area and may represent bounding structures of the graben system.

In the southeastern corner of the study area, a 1.5-m-high east-facing scarp extends across a Qfi surface and is characterized by a rounded crest and base (Sites 1, 2, and 5; Appendix A-1). The fault continues to the north, where it accommodates offset of a Qfo surface >3 m (Site 3; Appendix A-2). A splay of this fault with similar morphology and a scarp height of 2 m extends to the southwest of Site 1 across the Qfi surface (Sites 6 and 7; Appendix A-3). These scarps are shown on topographic profiles D and E (fig. 6). Both traces do not accommodate displacement of Qfy alluvium associated with Callaghan Creek south of the study area. Several discontinuous querried and approximately located faults are inferred to occur about 500 m west of these faults; however, these faults were difficult to follow in the field due to the deep dissection of the Qfo surface.

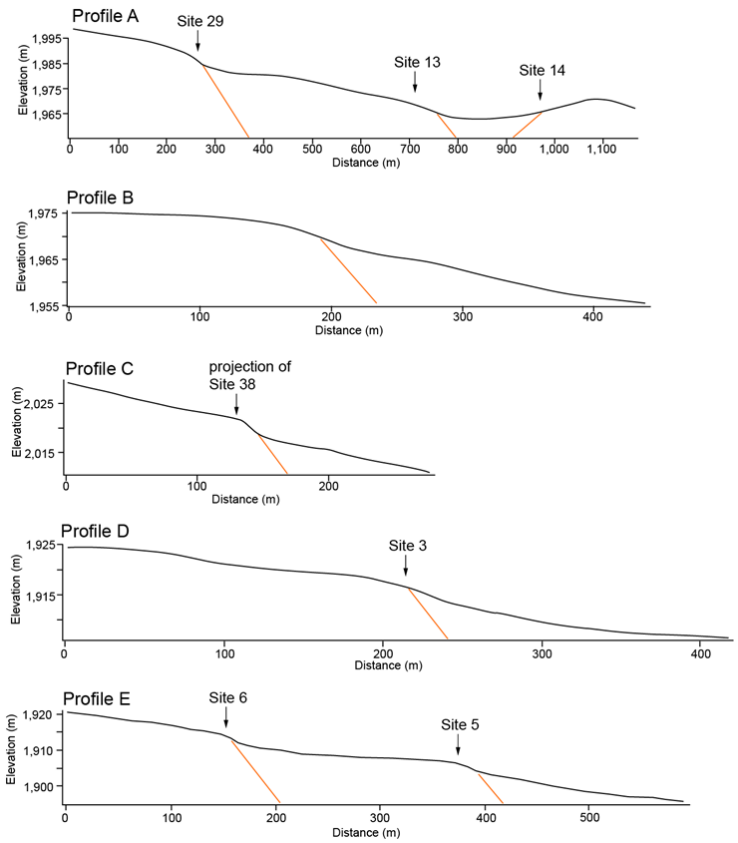

Figure 6. Topographic profiles (A–E) across tectonic scarps along the Mount Callaghan faults. Location of profiles shown on figure 5A. Red lines indicate schematic interpretations of faults at depth (dip is not constrained).

A prominent graben system extends across the south-central part of the study area (Sites 8–19) and is characterized by clear east- and west-facing scarps (fig. 5A; profile A, fig. 6). Long-term displacement across this structure is supported by bedrock offsets observed in the east-west trending ridge south of Callaghan Creek (Appendix A-4). North of Callaghan Creek at Site 8, the fault is subtly expressed by a 0.5-m-high west-facing scarp that has been partially buried by fan deposition. This scarp increases in height to the north to ~3 m at Site 11 (Appendix A-4). The east-dipping fault that bounds the western side of the graben extends between Sites 13 and 19 and is expressed as a 3-m-high scarp that splits into two closely spaced traces in a few locations (Site 16, Appendix A-5). North of Site 13, the graben widens to ~100 m. The northern projection of this fault is associated with an ~4-m-high scarp as shown on profile B (fig. 6). The graben extends across Qfi and Qfo surfaces, and Qfy surfaces that occupy incised channels are not offset.

Another east-facing fault occurs ~500 m upslope of the graben and extends along Sites 24–32 (fig. 5A, Appendices A-6 to A-8). This fault is continuous for at least 3 km and is associated with an ~4-m-high east-facing scarp in Qfo deposits that is characterized by rounded morphology. At Site 28, the fault is associated with a small (100 m) right step, where it projects into a Qfi surface. The Qfi surface is displaced ~1.5 m. This fault is crossed by profile A at Site 29 (fig. 6).

From the mouth of Callaghan Creek, a prominent east-dipping fault extends for at least 2 km north through Site 38, where it is expressed as a 2.5-m-high scarp across Qfi and possibly Qfy(?) surfaces (Appendix A-9). A small bedrock knob along the north bank of the creek is aligned with the scarp and has a distinct triangular facet shape. This scarp is shown on profile C (fig. 6). North of Site 38, the fault bends to the west and discontinuously follows the bedrock alluvial contact, where it is characterized by short weakly expressed lineaments. The range front here lacks tectonic geomorphic features (i.e. triangular facets) and is characterized by smooth eroded slopes (Appendix A-10). A secondary range front lineament (mapped as a querried fault) that extends along the western margin of the study area also lacks facets and may be related to bedrock discontinuity.

The fault that projects across the mouth of Callaghan Creek projects to the south into a prominent range-front

fault trace characterized by a sharp bedrock/alluvium contact, wine glass canyons, triangular facets, and oversteepened basal slopes (Site 40, Appendix A-11). These features are all indicative of active Quaternary displacement and suggest that this fault may be the master east-dipping structure of the Mount Callaghan fault system.

Two additional west-dipping faults occur in the northeastern part of the study area (Site 20) and were observed from a distance. These faults appear to displace Tertiary ash-flow tuff deposits. Analyses of the lidar DEM suggest that these faults may be associated with up to 10–15 m of displacement. A connection of these faults to the faults that extend across the piedmont slope to the south was not established; however, their sense of displacement suggests that they may be the expression of long-term graben formation.

In summary, tectonic geomorphic features are weakly expressed along the range front within the study area; however, faults are clearly expressed and well-defined in Quaternary deposits on the piedmont. Tectonic displacements across mapped faults that cut Qfo and Qfi surfaces on the piedmont range between 3 and >4 m and 0.5 and 2.5 m, respectively, and Qfy surfaces are not displaced. Based on the relative age of Qfy surfaces, the last surface-rupturing earthquake along the Mount Callaghan faults predates the latest Pleistocene. A prominent east-dipping range-front fault projects into the field area near the mouth of Callaghan Creek. The sum of observations suggests that this fault is the master fault of the Mount Callaghan fault system and that hanging-wall deformation is responsible for the wide zone of faults distributed across the piedmont in the study area.

DISCUSSION AND SUMMARY

This study included an evaluation of the tectonic geomorphology and the location and relative activity of the Mount Callaghan fault system along the eastern margin of the Toiyabe Range in southern Grass Valley, Lander County, Nevada. The mapping effort utilized high-resolution topographic data (lidar) and field reconnaissance to refine previous fault mapping. The results indicate that the Mount Callaghan faults have accommodated Quaternary displacement but have been relatively quiescent since the latest Pleistocene. The system consists of a prominent east-dipping range-front structure and a widely distributed zone of hanging wall faults and grabens that extend across the piedmont slope within the study area.

The Mount Callaghan faults occur within a complex tectonic setting including an intersection with the Simpson Park Mountains fault and a left-step from the Toiyabe Range fault. This area was defined as a favorable structural setting (accommodation zone) for geothermal power generation by Faulds et al. (2021), which was realized by the development McGinness Hills geothermal power plant. The Simpson Park Mountains, Toiyabe Range, and Mount Callaghan faults are all Quaternary active structures and associated with a broad region of microseismicity. The spatial correlation of aftershocks with gold mineralization (Cox and Ruming, 2004; Micklethwaite and Cox, 2004), as well as similarities in the geologic conditions that favor geothermal activity and gold mineralization suggest that the region surrounding the Mount Callaghan faults may be a location fruitful for future gold exploration.

The dip of the Mount Callaghan faults is an important parameter for structural modeling at depth; however, direct observations of the fault plane were not obtained, and the dip is uncertain. Frictional constraints associated with Andersonian mechanics (Anderson, 1951) suggest dips of 60° for normal faults consistent with relatively steep dips instrumentally recorded for historic earthquakes in the Great Basin (Doser, 1986). Relatively steep dips are also consistent with a dip of ~55° observed at an outcrop of the Toiyabe Range fault along U.S. Highway 50 south of the project area. Several investigations have focused on cumulative extension rates across parts of the Great Basin and have considered a range of dips for range-front faults between 30° and 60° degrees (Koehler, 2019; Wesnousky et al., 2005; Personius et al., 2017). Personius et al. (2017) determined that late Quaternary extension rates were equal to modern geodetic measures of extension if the faults dip ≤40° at seismogenic depths. Given the Mount Callaghan faults proximity to the 60° east-dipping Toiyabe fault and the ~8 km width of its graben system, it can be reasonably

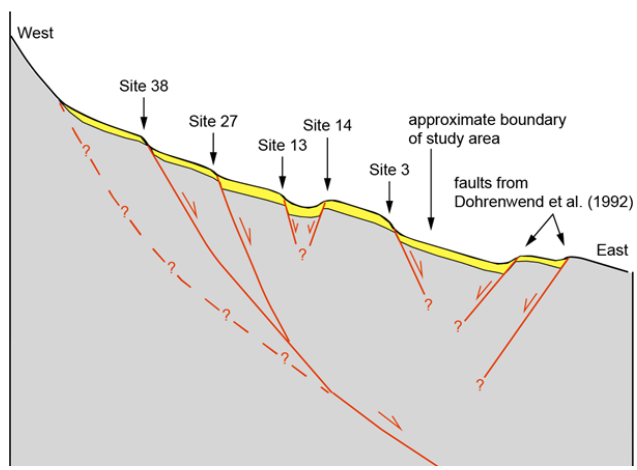

Figure 7. Schematic east-west cross section across the Mount Callaghan faults study area. Inferred faults shown by red lines. Dashed red line indicates inferred former location of a range-front structure implying that the active trace of the fault has migrated towards the basin. The dip of the main east-dipping fault shallows with depth potentially influencing the formation of grabens on the piedmont slope. Gray color is bedrock. Yellow color is alluvium. Not drawn to scale.

inferred that the main east-dipping range-front structure is relatively steep but likely shallows at depth beneath the piedmont slope. A schematic cross section showing these potential relations is shown on figure 7. Structural modeling of the Mount Callaghan faults would benefit from considering a range of dips including a relatively steep dip near the surface and moderate to shallow dips at depth.

CLOSURE AND LIMITATIONS

The results and conclusions presented in this report are based on evaluation of aerial photographs, satellite imagery, and lidar data, including lidar derivative map products (hillshade, slope, and surface roughness), as well as a two-day field reconnaissance. The field effort was limited to the southern part of the project area where road access was permitted. The mapped locations of Quaternary fault strands represent a refinement of previous mapping efforts; however, due to the complex system of grabens, the relative age of the fault scarps (>latest Pleistocene), and their subtle diffused morphology, additional traces likely exist. Bedrock mapping was not conducted as part of this project, and outcrops of faults in incised washes were not observed. Therefore, the dip of the faults at depth is uncertain.

ACKNOWLEDGMENTS

This project was supported through a research agreement between Renaissance Exploration, Inc. (Orogen Royalties) and University of Nevada, Reno. Gratitude is extended to Eli Turner of Renaissance Exploration, Inc. for assistance in coordinating project logistics, providing technical information and lidar data collected by NV5 Geospatial, and field access. Appreciation is also extended to Luke and Jessica Lancaster of Grass Valley Ranch for permission to access their property.

REFERENCES

Adams, K.D., Goebel, T., Graf, K., Smith, G., Camp, A.J., Briggs, R., Rhode, D.E., 2008, Late Pleistocene and early Holocene lake-level fluctuations in the Lahontan basin, Nevada—implications for the distribution of archaeological sites: Geoarchaeology, v. 23, no. 5, 608–643.

Anderson, J.G., Koehler, R.D., Abercrombie, R., Ahdi, S.K., Angster, S., Bormann, J., Brune, J.N., Dee, S.M., dePolo, C., Dickenson, S.E., Dunn, M., Faulds, J.E., Hammond, W.C., Hatch, R., Kell, A., Kent, G., Kreemer, C., Louie, J., Pierce, I., Ruhl, C.J., Smith, K.D., Taylor, W., Wesnousky, S.G., and Wong, I., 2019, A seismic hazards overview of the urban regions of Nevada—recent advancements and research directions: Seismological Research Letters, v. 90, no 4, p. 1577–1583.

Anderson, E.M., 1951, The dynamics of faulting: Edinburgh, Oliver and Boyd, 206 p.

Angster, S.J., Wesnousky, S.G., Figueiredo, P.M., Owen, L.A., and Hammer, S.J., 2019, Late Quaternary slip rates for faults of the central Walker Lane (Nevada, USA)—spatiotemporal strain release in a strike-slip fault system: Geosphere, v. 15, no. 5, p. 1460–1478.

Beroza, G.C., and Zoback, M.D., 1993, Mechanism diversity of the Loma Prieta aftershocks and mechanisms for mainshock-aftershock interaction: Science, v. 259, p. 210–213.

Cox, S.F., 2005, Coupling between deformation, fluid pressures, and fluid flow in ore-producing hydrothermal systems at depth in the crust: Economic Geology 100th Anniversary Volume, p. 1–35.

Cox, S.F., and Ruming, 2004, The St. Ives mesothermal gold system, western Australia—a case of golden aftershocks?: Journal of Structural Geology, v. 26, p. 1109–1125.

Dohrenwend, J.C., Schell, B.A., and Moring, B.C., 1992, Reconnaissance photogeologic map of young faults in the Millett 1° by 2° quadrangle, Nevada: U.S. Geological Survey Miscellaneous Field Studies Map MF-2176, 1 sheet, scale 1:250,000.

Doser, D.I., 1986, Earthquake processes in the Rainbow Mountain-Fairview Peak-Dixie Valley, Nevada region 1954–1959: Journal of Geophysical Research, v. 91, p. 12,572–12,586.

Eisenlohr, B.N., Groves, D., and Partington, G.A., 1989, Crustal-scale shear zones and their significance to Archean gold mineralization in western Australia: Mineralium Deposita, v. 24, p. 1–8.

Faulds, J.E., Coolbaugh, M.F., and Hinz, N.H., 2021, Inventory of structural settings for active geothermal systems and late Miocene (~8 Ma) to Quaternary epithermal mineral deposits in the Basin and Range Province of Nevada: Nevada Bureau of Mines and Geology Report 58, 27 p.

Hammond, W.C., and Thatcher, W., 2004, Contemporary tectonic deformation of the Basin and Range Province, western United States: 10 years of observation with the Global Positioning System—journal of Geophysical Research, v. 109, B08403.

Hammond, W.C., Blewitt, G., and Kreemer, C., 2014, Steady contemporary deformation of the central Basin and Range Province, western United States: Journal of Geophysical Research, v. 119, p. 5235–5253.

Hatem, A.E., Collett, C.M., Briggs, R.W., Gold, R.D., Angster, S.J., Powers, P.M., Field, E.H., Anderson, M., Ben-Horin, J.Y., Dawson, T., DeLong, S., DuRoss, C., Thompson Jobe, J., Kleber, E., Knudsen, K.L., Koehler, R.D., Koning, D., Lifton, Z., Madin, I., Mauch, J., Morgan, M., Pearthree, P., Pollitz, F., Scharer, K., Sherrod, B., Stickney, M., Wittke, S., and Zachariasen, J., 2022, Earthquake geology inputs for the U.S. National Seismic Hazard Model (NSHM) 2023 (western US) (ver. 2.0, February 2022): U.S. Geological Survey data release, https://doi.org/10.5066/P9AU713N.

Kilb, D., and Rubin, A.M., 2002, Implications of diverse fault orientations imaged in relocated aftershocks of the Mount Lewis, ML 5.7, California earthquake: Journal of Geophysical Research, v. 107, B11, doi:10.1029/2001JB000149, 17 p.

Koehler, R.D., 2019, Active faulting in the North Valleys region of Reno, Nevada: A distributed zone within the northern Walker Lane: Geomorphology, v. 326, p. 38–53.

Koehler, R.D., and Wesnousky, S,G., 2011, Late Pleistocene regional extension rate derived from earthquake geology of late Quaternary faults across Great Basin, Nevada between 38.50 and 400 N latitude: Geological Society of America Bulletin, v. 123, no. 3-4, p. 631–650.

Koehler, R.D., 2009, Late Pleistocene regional extension rate derived from earthquake geology of late Quaternary faults across Great Basin, Nevada between 38.5^0 and 40^{0}N latitude: University of Nevada Reno, Ph.D. dissertation, 242 p.

Micklethwaite, S., 2007, The significance of linear trends and clusters of fault-related mesothermal lode gold mineralization: Economic Geology, v. 102, p. 1157–1164.

Micklethwaite, S., and Cox, S.F., 2004, Fault-segment rupture, aftershock-zone fluid flow, and mineralization, Geology: v. 32, p. 813–816.

Micklethwaite, S., and Cox, S.F., 2006, Progressive fault triggering and fluid flow in aftershock domains—examples from mineralized Archaean fault systems: Earth and Planetary Science Letters, v. 250, p. 318–330.

Personius, S.R., Briggs, R.B., Maharrey, J.Z., Angster, S.J., Mahan, S.A., 2017, A paleoseismic transect across the northwestern Basin and Range Province, northwestern Nevada and northeastern California, USA: Geosphere, v. 13, no. 3, p. 782–810.

Roberts, R.J., Lehner, R.E., and Bell, M.M., 1963, Geologic map of Eureka County, Nevada: Nevada Bureau of Mines, Bulletin 64, plate 3, scale 1:250,000.

Schell, B.A., 1981, Faults and lineaments in the MX Siting Region, Nevada and Utah, Volume II: Technical report to U.S. Department of [Defense] the Air Force, Norton Air Force Base, California, under Contract FO4704-80-C-0006, November 6, 1981, 29 p., 11 pls., scale 1:250,000.

Sibson, R.H., Robert, F., and Poulsen, K.H., 1988, High-angle reverse faults, fluid pressure cycling, and mesothermal gold deposits: Geology, v. 16, p. 551–555.

SRTM, 2013, NASA Shuttle Radar Topography Mission (SRTM) Global. Distributed by OpenTopography, https://doi.org/10.5069/G9445JDF. Accessed: 2022-11-10.

Stewart, J.C., and McKee, E.H., 1968, Geologic map of the Mount Callaghan quadrangle, Lander County, Nevada: U.S. Geological Survey Geologic Quadrangle Map GQ-730, 1 sheet, scale 1:62,500.

Stewart, J.H., and Carlson, J.E., 1976, Geologic map of north-Central Nevada: Nevada Bureau of Mines and Geology Map 50, scale 1:250,000.

Stewart, J.H., and McKee, E.H., 1977, Geology and mineral deposits of Lander County, Nevada: Nevada Bureau of Mines and Geology Bulletin 88, 3 plates, 106 p.

U.S. Geological Survey (USGS), 2022, Quaternary fault and fold database for the United States, accessed November 1, 2022.

Wesnousky, S.G., Barron, A.D., Briggs, R.W., Caskey, J.S., Kumar, S., Owen, L., 2005, Paleoseismic transect across the northern Great Basin, USA: Journal of Geophysical Research v. 110 (B05408).

APPENDIX

Appendix A. Photographs and details from selected field observation sites.

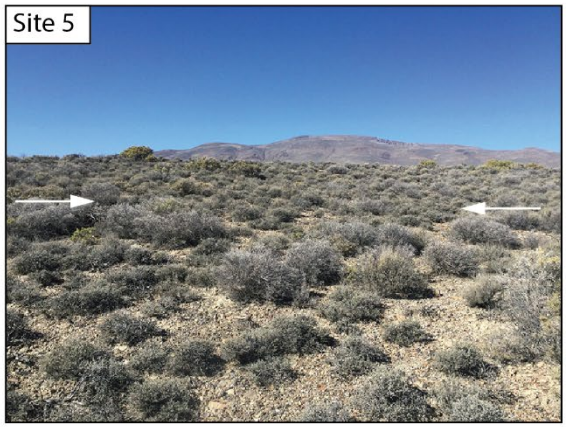

A-1. Photographs of ~1.5-m-high east-facing scarp across Qfi surface at Sites 1 (left) and Site 5 (right). Scarp extends between white arrows in each photo. Views to west.

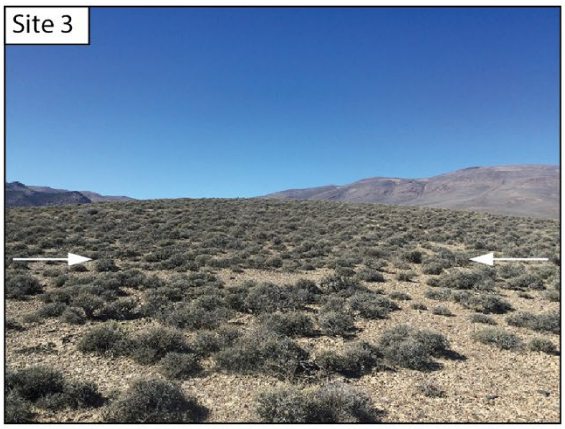

A-2. Photograph of ~3.5-m-high east-facing scarp across Qfo surface at Site 3. Scarp extends between white arrows. View to west.

A-3. Photographs of ~2-m-high east-facing scarp across Qfi surface at Site 6 (left) and Site 7 (right). At Site 7 truck is parked on the hanging wall. Dirt road extends across scarp. Scarp extends between white arrows in each photo. Views to west.

Appendix A. Photographs and details from selected field observation sites.

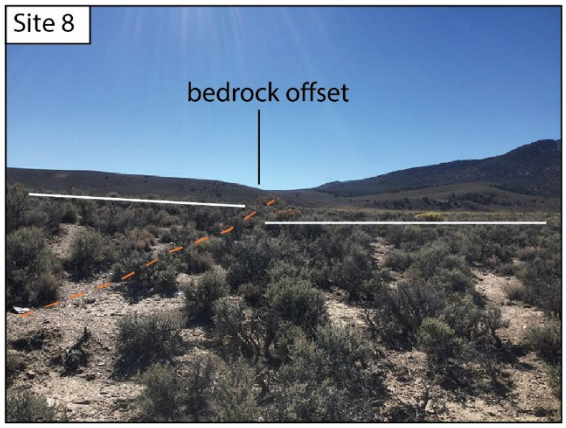

A-4. (left) Photograph of ~0.5-m-high west-facing scarp across Qfi surface at Site 8. White lines indicate top of surface, fault indicated by dashed red line. View to south. (right) Photo of west-facing ~3-m-high scarp at Site 11. Fault extends between white arrows. View to east.

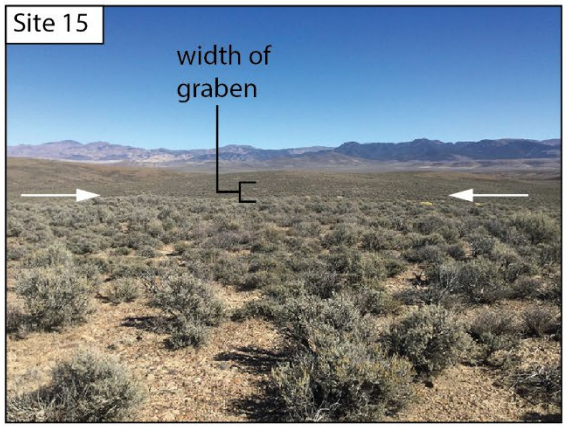

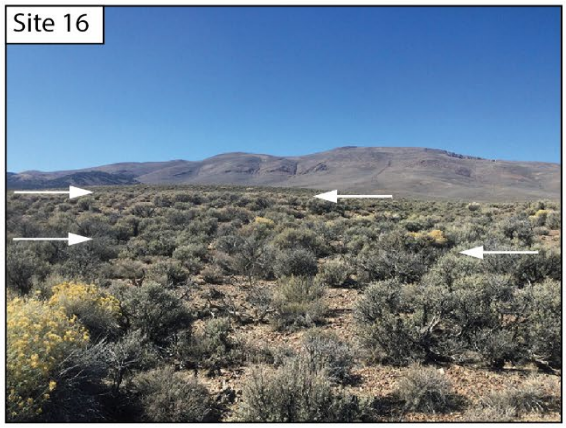

A-5. (left) Photograph of large graben (white arrows) extending across Qfo surface. View to east. (right) Photograph of parallel east-facing fault traces bounding west side of graben. Faults extend between white arrows. View to west.

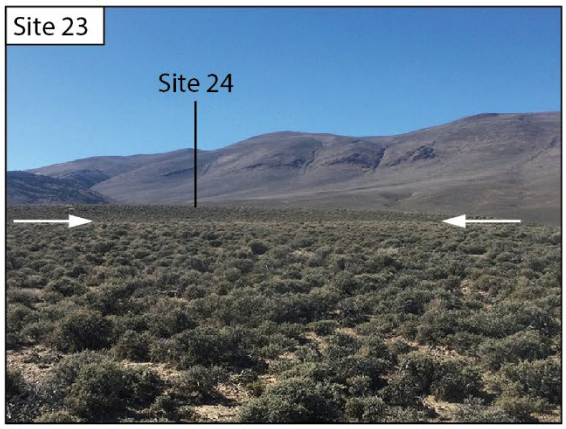

A-6. Photograph of ~4-m-high east-facing scarp across Qfo surface. Fault extends between white arrows. View west towards Site 24.

Appendix A. Photographs and details from selected field observation sites.

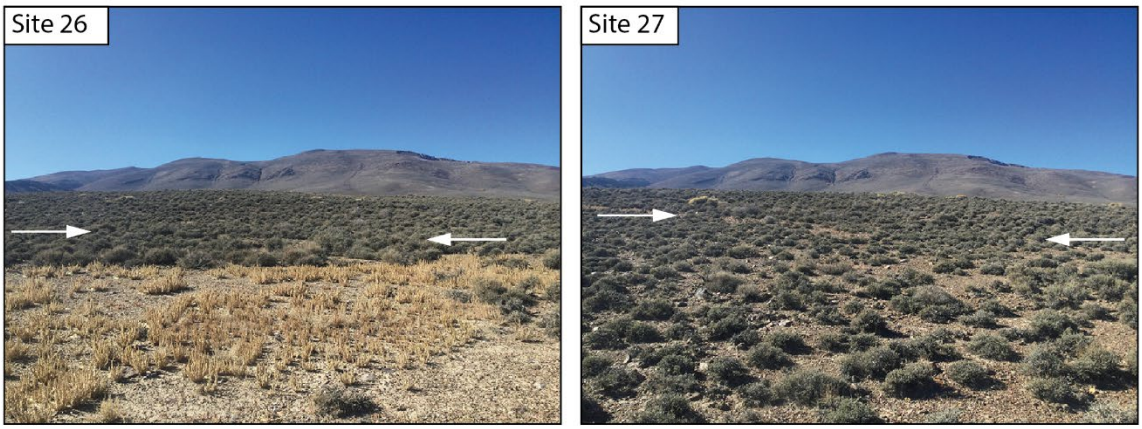

A-7. Photographs of ~4-m-high east-facing scarp across Qfo surface at Sites 26 (left) and 27 (right). Fault extends between white arrows in both photos. View to west.

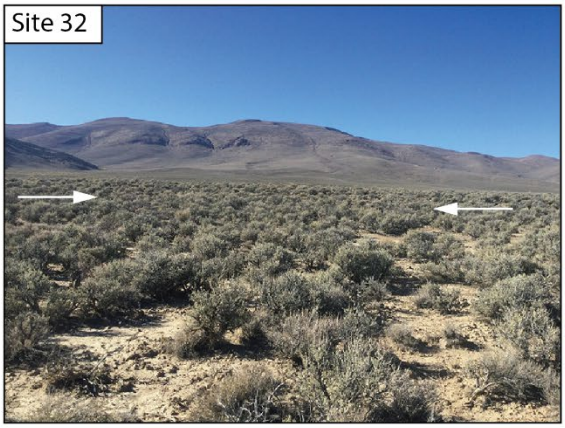

A-8. Photograph of east-facing ~1.5-m-high scarp across Qfi surface at Site 32. Fault extends between white arrows. View to west.

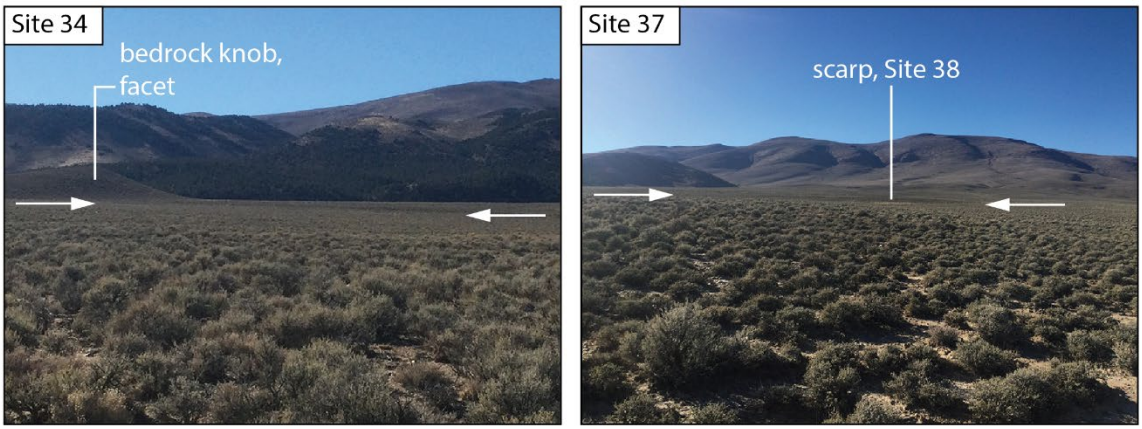

A-9. Photographs of east-facing scarp that projects to the south towards prominent range front scarp. Views to west. (left) View from Site 34 showing triangular facet across a bedrock knob and backlit scarp. (right) View from Site 37 towards scarp at Site 38. Fault extends between white arrows in both photos.

Appendix A. Photographs and details from selected field observation sites.

A-10. Photographs taken from Site 39 showing the lack of tectonic geomorphic features indicative of active deformation along the eastern flank of Mt. Callaghan. View to west.

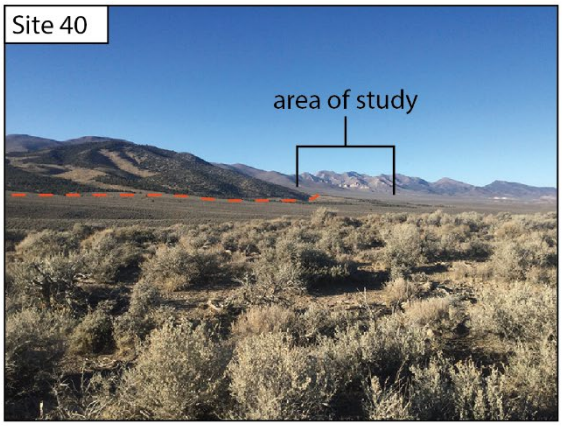

A-11. Photograph taken from Site 40 south of the study area showing prominent range-front fault trace (red dashed line) that projects towards the Mount Callaghan faults. View to west.

Nevada Bureau of Mines and Geology

nbmg.unr.edu

University of Nevada, Reno